Accepted Manuscript

Controlling particle size in the Stöber process and incorporation of calcium

Sarah L. Greasley, Samuel J. Page, Slobodan Sirovica, Shu Chen, Richard A. Martin, Antonio Riveiro, John V. Hanna, Alexandra E. Porter, Julian R. Jones

PII: S0021-9797(16)30066-2
DOI: http://dx.doi.org/10.1016/j.jcis.2016.01.065
Reference: YJCIS 21048

To appear in: *Journal of Colloid and Interface Science*

Received Date: 23 August 2015
Revised Date: 26 January 2016
Accepted Date: 27 January 2016

Please cite this article as: S.L. Greasley, S.J. Page, S. Sirovica, S. Chen, R.A. Martin, A. Riveiro, J.V. Hanna, A.E. Porter, J.R. Jones, Controlling particle size in the Stöber process and incorporation of calcium, *Journal of Colloid and Interface Science* (2016), doi: http://dx.doi.org/10.1016/j.jcis.2016.01.065

Controlling particle size in the Stöber process and incorporation of calcium

Sarah L. Greasley[1*], Samuel J. Page[2], Slobodan Sirovica[3], Shu Chen[1], Richard A. Martin[3], Antonio Riveiro[1,4], John V. Hanna[2], Alexandra E. Porter[1], Julian R. Jones[1]

[1]Department of Materials, Imperial College London, UK, s.greasley12@imperial.ac.uk
[2]Department of Physics, University of Warwick
[3]School of Engineering & Applied Science and Aston Research Centre for Healthy Ageing, University of Aston
[4]Applied Physics Department, University of Vigo, E.I.I., Lagoas-Marcosende E-36310, Vigo, Spain

Abstract

The Stöber process is commonly used for synthesising spherical silica particles. This article reports the first comprehensive study of how the process variables can be used to obtain monodispersed particles of specific size. The modal particle size could be selected within in the range 20 – 500 nm. There is great therapeutic potential for bioactive glass nanoparticles, as they can be internalised within cells and perform sustained delivery of active ions. Biodegradable bioactive glass nanoparticles are also used in nanocomposites. Modification of the Stöber process so that the particles can contain cations such as calcium, while maintaining monodispersity, is desirable. Here, while calcium incorporation is achieved, with a homogenous distribution, careful characterisation shows that much of the calcium is not incorporated. A maximum of 10 mol% CaO can be achieved and previous reports are likely to have overestimated the amount of calcium incorporated.

Key Words

Stöber process; bioactive glass; nanoparticles; biodegradable; sol-gel

1. Introduction

Bioactive glass nanoparticles have great potential for delivery of therapeutic cations and they can be made by sol-gel [1]. Bioactive glasses can act as delivery vehicles for sustained delivery of active ions that have therapeutic benefit [2]. The benefit of biodegradable glasses over polymers is that the ions are incorporated into the glass composition, due to the amorphous structure, and they are released at a sustained rate as the glass dissolves [3]. Nanoparticles have particular benefit for intracellular delivery of ions [1]. Sol-gel processing methods are used to produce silica networks by hydrolysis and condensation reactions [4]. A benefit over melt-quench glasses is that there is potentially more control over composition at lower processing temperatures. A silicate precursor is required, which typically takes the form of a silicon alkoxide, such as tetraethyl orthosilicate (TEOS). Silicon alkoxides hydrolyse under both acidic and basic conditions, after which polycondenation occurs and Si-O-Si bonds start to form, creating a sol of dispersed nanoparticles. In the acid-catalysed system, particles aggregate as condensation continues to form a three-dimensional gel network [4, 5]. However, under basic conditions, the presence of OH^- ions results in repulsive forces making it possible to synthesise monodispersed spherical nanoparticles [6]. Stöber pioneered this system, producing monodisperse silica spheres in the micron size range (from 0.05 – 2 μm) [6].

The Stöber process is simple: Tetraethyl orthosilicate (TEOS) is added to a solution of water, alcohol and ammonium hydroxide under agitation. One of the advantages of the method is the ability to control particle size, distribution and morphology by systematic variation of reaction parameters [7]. Other papers have been published on the synthesis of silica micro- and nanoparticles and have adapted the Stöber process with various concentrations in their own investigations [8-16]. However, the synthesis methods have become increasingly complex with no clear benefits. The process's high sensitivity to the effects of temperature, pH and reactant

concentrations have affected reproducibility and consistent trends have not always been observed [10, 14]. Whilst there have been attempts to demonstrate how each of these variables affects the final particle properties, most papers use different concentrations and processing methods, making comparison difficult. There is still much disagreement in the field and the original paper published by Stöber *et al.* [6] and that of Bogush *et al.* [8] remain the most comprehensive studies. The aim here is to incorporate cations in the Stöber process while maintaining monodispersity in nanoparticles. In order to do that, it was first necessary to gain a comprehensive understanding of the effects of variables in the Stöber process.

It is well known that the sol chemistry affects the rates of hydrolysis and condensation, which in turn affects nucleation, aggregation and growth of particles [4, 12]. It is proposed that particle growth follows a nucleation and aggregation mechanism [4, 17], in which initial negatively charged particles (<10 nm) are unstable due to their size, resulting in aggregation and a collective reduction in surface area. Competition between nucleation and aggregation is dependent on reactant concentrations and has a large effect on final particle properties such as size [18]. Uniformity in particle size can be achieved with this mechanism as a result of size dependent aggregation rates [8, 18] determined by colloid interaction potentials. The aggregation rate is fastest between small-large particles and slowest between large-large particles [18]. Initial particles restructure through Ostwald ripening, in which aggregates dissolve and then reprecipitate, consuming smaller particles to form larger more stable ones. However, Ostwald ripening cannot account for the rapid growth of particles in the 45 - 250 nm range. The most likely mechanism for the growth of larger particles is by reaction-limited monomer-cluster growth (RLMCA) [4], where the probability of monomer attachment is governed by local structure. There are many collisions between monomer (a silicate tetrahedron in this case) and cluster before a bond is formed, with all potential growth sites being sampled by the monomer. In basic conditions, all cluster sites are reactive and occupied with equal probability, therefore giving rise to spherical particles [4]. It is predicted that RLMCA occurs on two length scales with the smaller particles now acting as monomers [4]. This mechanism is supported by Feeney *et al.* [17], Lee *et al.* [18] and Harris *et al.* [13]. Once the soluble silica concentration has dropped below the critical nucleation concentration, it is hypothesised that monomer addition subsequently occurs on the surface of the aggregated particles in accordance with LaMer and Dinegar's theory of monomer addition [19], leading to smoothing of the colloid surface [8, 12, 16].

The incorporation of calcium into the nanoparticles is desirable in order to create a bioactive system. Soluble silica and calcium ion release stimulates cells at a genetic level causing osteogenic cells to produce bone matrix [2, 20, 21]. The addition of calcium also increases glass dissolution by acting as a network modifier. Bioactive glass nanoparticles can also be incorporated into nanocomposites [22]. Whilst the synthesis of monodispersed Stöber silica nanoparticles has been achieved previously in literature, the addition of calcium significantly complicates the procedure and can cause the particles to become irregular in morphology [23] or to agglomerate [24-26]. While nominal compositions of particles are quoted in the literature, the final compositions are rarely ratified by analytical techniques or only non-quantitative energy-dispersive X-ray spectroscopy (EDX) data is provided [3, 25, 27].

One of the reasons for the challenges in incorporating calcium into the silicate network is that it requires elevated temperature when calcium salts are used as the calcium precursor. Several groups have attempted to incorporate calcium into silica nanoparticles by using a two-step sol-gel process in which precursors of silica and calcium (TEOS and calcium nitrate respectively) are hydrolysed in an acidic solution before gelation under alkaline conditions [24-28]. While EDX data showed calcium was present in the particles [25] and they induced HCA formation in simulated body fluid (SBF), little or no quantitative analysis was performed on the final elemental composition. The particles are also seen to be aggregated and irregular in both size and shape [24, 25, 27]. Labbaf *et al.* incorporated calcium by adapting the process used by Zhao *et al.* [29] in which Boltorn™ polymer was used as a template in the sol-gel process before being burnt out during calcination. The submicron particles were shown to be of composition 86 mol% SiO_2 and 14 mol% CaO, verified by quantitative inductively coupled plasma optical emission spectroscopy (ICP) analysis [23]. However, despite being spherical and dispersed, the resulting particles did not show a homogeneous size distribution even after optimisation of the polymer:TEOS ratio. Some papers have attempted to improve the dispersion or shape of the nanoparticles by

use of a surfactant [25, 28]. However, this can inhibit calcium diffusion, therefore limiting the amount of calcium that enters the glass [1].

Calcium nitrate is usually used as the calcium source in the sol-gel synthesis of bioactive glass, but the calcium is not incorporated into the silicate network until it is heated to above 400˚C [5]. Before drying, the calcium nitrate is dissolved in the sol, however, as the particles are dried it precipitates onto the surface of the silica particles. Before the addition of calcium, Nuclear Magnetic Resonance (NMR) data shows that the silica network is highly connected. However, once 400˚C is reached, the calcium diffuses into the silica particles and becomes a network modifier, reducing network connectivity [5]. Excess Ca^{2+} on the surface of the particles may change the surface charge and cause the agglomerated particles seen in literature. Tsigkou *et al.* found the ratio of Si:Ca to be a critical factor in producing monodispersed particles [1]. They also found that particles of ~230 nm were internalised by bone marrow derived stem cells (MSCs) and fat derived stem cells (ADSCs) without causing toxicity or differentiation, even when the particles degraded inside the cells. Understanding the mechanism of calcium incorporation means that it is not necessary to have calcium in the sol from the start of the process. De Oliveira *et al.* [30] synthesised silica nanoparticles using a modified version of the Stöber process, including phosphate, before filtering the sol and subsequently adding calcium nitrate, but they did not achieve a homogeneous distribution of particles. One possible way of increasing the amount of calcium that can be incorporated would be by use of an alternative calcium source. Other potential calcium sources that have been investigated are calcium chloride and calcium methoxyethoxide (CME). Calcium chloride was not incorporated into the network at any of the temperatures investigated resulting in extremely high percentages of Q^4 groups [31]. The CME alkoxide on the other hand, was found to incorporate into the network at low temperatures, making it an excellent alternative to calcium salts. However, it is highly reactive in comparison with the silica precursor TEOS, meaning that as it gels immediately on contact with water, making the production of nanoparticles difficult [31].

The objectives of this paper were to:

i) Revisit the original Stöber process to provide a comprehensive understanding of how to reliably control particle size, whilst maintaining monodispersed particles;
ii) Investigate the subsequent incorporation of calcium with complete quantitative characterisation of the nanoparticles to prove the incorporation of calcium, with the 70S30C composition (70 mol% SiO_2, 30 mol% CaO) [32-34] as the target value;
iii) Assess the dissolution of the particles in artificial lysosomal fluid (ALF) and Simulated Body Fluid (SBF) to determine how they might degrade in the body.

2. Experimental

2.1. Particle Synthesis

All reagents were purchased from Sigma-Aldrich. Using the original Stöber process [6], ethanol (ethyl alcohol, 200 proof, ≥99.5%), distilled water, and ammonium hydroxide (ACS reagent, 28.0-30.0% NH_3 basis) were mixed in an ultrasonication bath at room temperature. After 10 minutes, TEOS (tetraethyl orthosilicate, reagent grade, 98%) was added to the solution and the solution was left overnight, or until the particles had reached maximum size (determined by dynamic light scattering, DLS). A TEOS concentration of 0.28 M was used (as per the Stöber process) with a range of water concentrations from 3 - 15 M and ammonium hydroxide concentrations varying from 0.11 – 1.13 M. TEOS concentrations of 0.045M, 0.17M and 0.5M were later analysed as these have been also used in previous papers [6, 8, 15, 35].

The solution was then centrifuged to obtain a solid pellet of particles, which was dried overnight at 60˚C. Removal of solution by centrifugation was performed due to reports that drying in the presence of water can result in agglomeration phenomena caused by condensation reactions at inter-particle contacts [7].

For particles containing calcium, monodispersed silica particles were first synthesised using the method described. However, after centrifugation, the particles were redispersed in distilled water and calcium nitrate

tetrahydrate (ACS reagent, 99%) was added to the solution. After 20 minutes, the particles were centrifuged again, the supernatant was removed and the pellet was dried at 60˚C overnight as before. The particles were then heated to 680˚C for 3 h, at a heating rate of 3˚/min. 680˚C was chosen to allow for the removal of nitrates and incorporation of calcium into the network, without crystallisation [5, 23]. Subsequently the particles were washed 3 times in ethanol to remove any excess calcium not incorporated into the network. It was predicted that the use of this two-step process would allow for the homogeneity and size control of nanoparticles created using the Stöber process to be maintained.

Investigations were also carried out into the viability of increasing the mol% of calcium in the particles by increasing the amount of calcium nitrate added to the solution. 6 molar ratios of Ca:Si were investigated 15:85, 30:70, 1:1, 1.3:1, 2:1 and 4:1.

2.2. Particle characterisation

Particle size of each sample was determined by diluting samples with ethanol and using dynamic light scattering (DLS, Malvern instrument 2000). Stöber particles have extremely high colloidal stability and low absorption at 633 nm making DLS suitable. However, DLS inherently calculates the hydrodynamic radius of particles giving slightly larger values [36].

Particles were also imaged using bright field transition electron microscopy (TEM). For TEM analysis, the samples were collected on 300 mesh copper TEM grids coated with holey carbon film and imaging was performed on a JEOL-2000FX TEM using an operating voltage of 200 kV and a 10 µm objective aperture to increase mass-thickness contrast. Multiple areas of each grid were analysed and 100 particles from each sample were measured to calculate a mean particle diameter and standard deviation.

After calcium incorporation, the particles were again analysed using TEM and DLS. The composition of the particles produced was also determined using the quantitative method of acid digestion and inductively coupled plasma optical emission spectroscopy (ICP-OES, Thermo Scientific ICap 6000series). Nanoparticle composition was additionally characterised by X-ray fluorescence (XRF) spectroscopy using a Siemens SRS 3000 unit equipped with an Rh anode and a 60 kV X-ray generator. A Field Emission Gun Scanning Electron Microscope (FEG-SEM JEOL JSM 6700F) equipped with an Energy-dispersive X-ray spectroscopy (EDS) detector (Oxford Inca Energy 300) was also used to perform semi-quantitative analysis. Elemental standards were used as follows: C: $CaCO_3$; Si: SiO_2; Al: Al_2O_3; O: SiO_2; Ca: $CaSiO_3$, and EDS scans were obtained at 5 random points in each the sample to obtain average elemental ratios.

Further investigation into the atomic structure of the particles was carried out using X-ray scattering to determine whether any crystalline phases were present and to show the decomposition of calcium nitrates after heat treatment. X-ray data was collected at the BM28 at the European Synchrotron Radiation Facility (ESRF), Grenoble, France. Measurements were performed with a monochromatic (λ=0.827Å, E=15.039keV) incident X-ray beam of cross section 0.8 by 0.5 mm. Samples were mounted inside a brass annulus (1cm diameter x 1mm thickness) contained in a thin Mylar envelope. A MAR CCD (2048 by 2048 pixels) was positioned behind the sample and orthogonal to the incident beam to collect scattering data. The sample holder was positioned 30 cm from the beam source and 57 cm from the detector window to provide a Q range of 0.4 to 1.9 $Å^{-1}$, where $Q = 4\pi \sin\theta/\lambda$. Measurements were undertaken on the samples, empty container, direct beam, water and calibration standard to allow the diffraction patterns to be corrected for background and normalisation effects. The data was normalised and background corrected using the Fit2D software package [37]. Data was radially averaged over 360° to produce a 1D output and were subsequently fitted with Gaussian models to determine peak positions.

For the first time, particles were also sectioned using a dual beam Focused Ion Beam Scanning Electron Microscope FIB-SEM (FEI Helios 600 NanoLab). EDS on a JEOL-2100F TEM with AZtec imaging software was used to map the elements present through the cross section of the particles. The EDS detector was an Oxford Instrument system, X-Max 80 mm Silicon Drift Detector (SDD) and the TEM 2100F was operated at 200 kV accelerating voltage.

Magic Angle Spinning ^{29}Si Solid State Nuclear Magnetic Resonance (MAS NMR) was performed to determine the effect of calcium addition on silicate bonding and network connectivity, which can be used as an indication of network disruption by the calcium and potential bioactivity. ^{29}Si single pulse MAS NMR measurements were performed at 7.0 T using a Varian/Chemagnetics InfinityPlus spectrometer operating at a Larmor frequency of 69.62 MHz. These experiments were performed using a Bruker 7 mm HX probe which enabled a MAS frequency of 5 kHz to be implemented. Flip angle calibration was performed on kaolinite from which a $\pi/2$ pulse time of 5.5 μs was measured. All measurements were undertaken with a $\pi/2$ tip angle along with a delay between subsequent pulses of 240 s. All ^{29}Si centre of gravity (apparent) shifts were reported against the IUPAC recommended primary reference of Me_4Si (1% in $CDCl_3$, δ 0.0 ppm), via a kaolinite secondary in which the resonance is a known shift of -92.0 ppm [38].

2.3. Dissolution studies

Nanoparticles < 250 nm are likely to be internalised by cells after which the vesicle they are contained within fuses with a lysosome [1]. A protocol was therefore developed for performing a dissolution study on the nanoparticles in ALF over a time period of 2 weeks, based on experiments previously conducted by Bailey *et al.* [39]. ALF was prepared in accordance with previous work [40]. 75 mg of bioactive glass nanoparticles were suspended in 3 ml of ALF (pH 4.5). The solution was placed in SnakeSkin Dialysis Tubing (3.5K MWCO, 16 mm dry I.D) and placed in a pot made up with ALF solution to a final volume of 50 ml. All samples were incubated at 37 °C in an orbital shaker at 120 rpm. Aliquots of 1 mL were taken at 1, 2, 4, 6, 8 24, 48, 72 h from the bulk solution and replaced with 1 mL of fresh ALF. Samples collected at each time point were then diluted with 2M HNO_3 for ICP analysis. A dissolution study was also performed in SBF, in the same way, to simulate the initial extracellular environment to which the nanoparticles would be exposed. SBF was prepared in accordance with Kokubo *et al.* [41].

3. Results and discussion

3.1. Stöber process revisited

Initially, Stöber silica particles were synthesised and a comprehensive study of the processing variables carried out. Figure 1A shows particle size results from DLS, as a function of water and ammonium hydroxide content. Increasing ammonium hydroxide concentration resulted in increased particle size. This trend was also confirmed by TEM images shown in Figure 2. The role of ammonium hydroxide in the process is to raise the pH, which accelerates the polycondensation reaction but also creates an environment with a pH much higher than the isoelectric point, which for silicic acid in aqueous solution is 2.2, creating repulsive charges between the particles, critical for monodispersity [4, 12]. At all ammonium hydroxide concentrations, as water concentration increased from 3 – 15 M, particle size initially increased to a maximum at 9 M H_2O before decreasing. This trend was most significant at higher ammonium hydroxide concentrations (0.85 M and 1.13 M) and is again confirmed by TEM images (Figure 3). Figure 1A indicates that particle size could be controlled from 20.5±1.7 nm (3 M H_2O, 0.11 M NH_4OH) to 823.8±122.4 nm (9 M H_2O, 1.13 M NH_4OH), according to DLS. The DLS values quoted are the number mean. Figure 2B shows that the particle size distribution was narrowest when particles were smallest, e.g. with a polydispersity index (PDI) of 0.012 for 6 M H_2O, 0.11 M NH_4OH, and that the width of the distributions increased as the particle size and ammonium hydroxide concentration increased, e.g. PDI increased to 0.021 at 1.13 M NH_4OH. However, TEM images showed good monodispersity for all concentrations (Figure 2). In fact, as a percentage of particle size, the standard deviation decreased as particle size increased, as seen in previous studies [8, 16, 42].

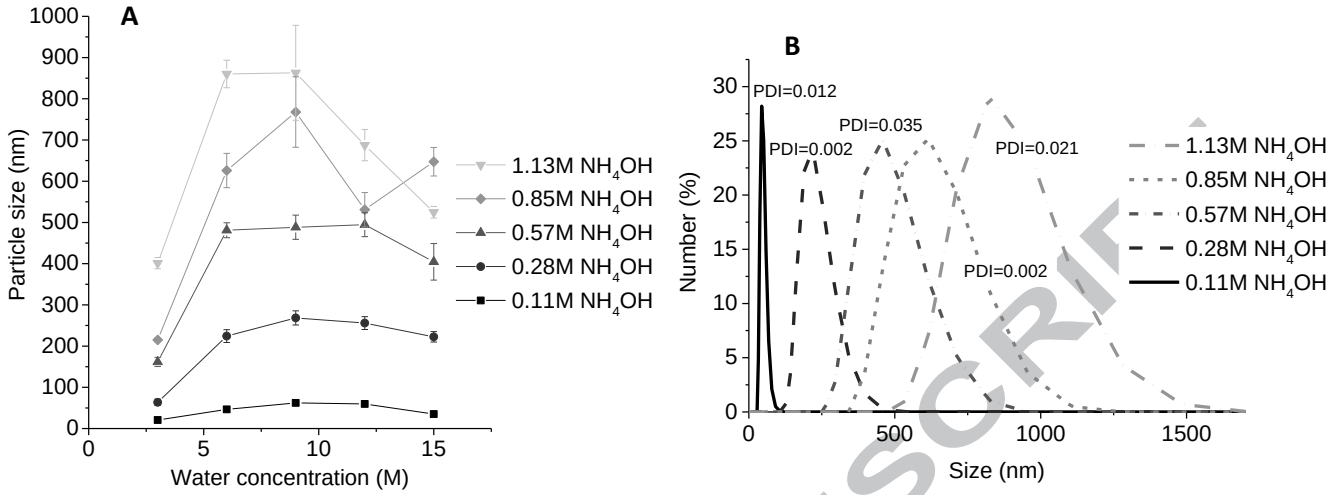

Figure 1. A) Mean particle size of silica particles (DLS number mean) as a function of water and ammonium hydroxide concentration for 0.28 M TEOS. Error bars show the standard deviation from the mean (n=3). B) Example DLS distributions with increasing ammonium hydroxide concentrations for 0.28M TEOS and 6M H_2O.

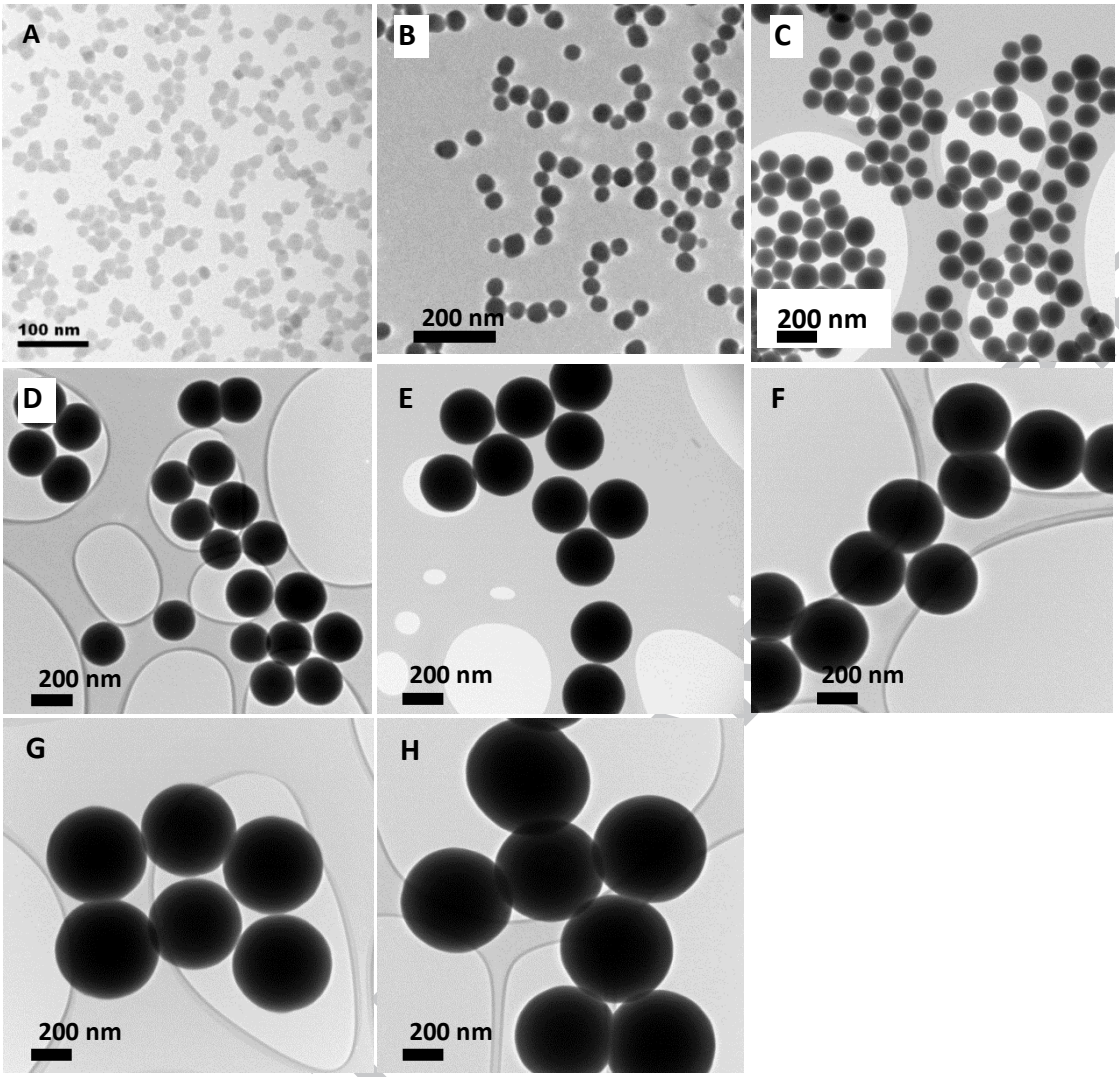

Figure 2. TEM images of silica particles produced using 0.28 M TEOS, 6 M H_2O and varying concentrations of ammonium hydroxide: A) 0.056 M NH_4OH B) 0.11 M NH_4OH C) 0.17 M NH_4OH D) 0.28 M NH_4OH E) 0.40 M NH_4OH F) 0.57 M NH_4OH G) 0.8 5M NH_4OH H) 1.13 M NH_4OH.

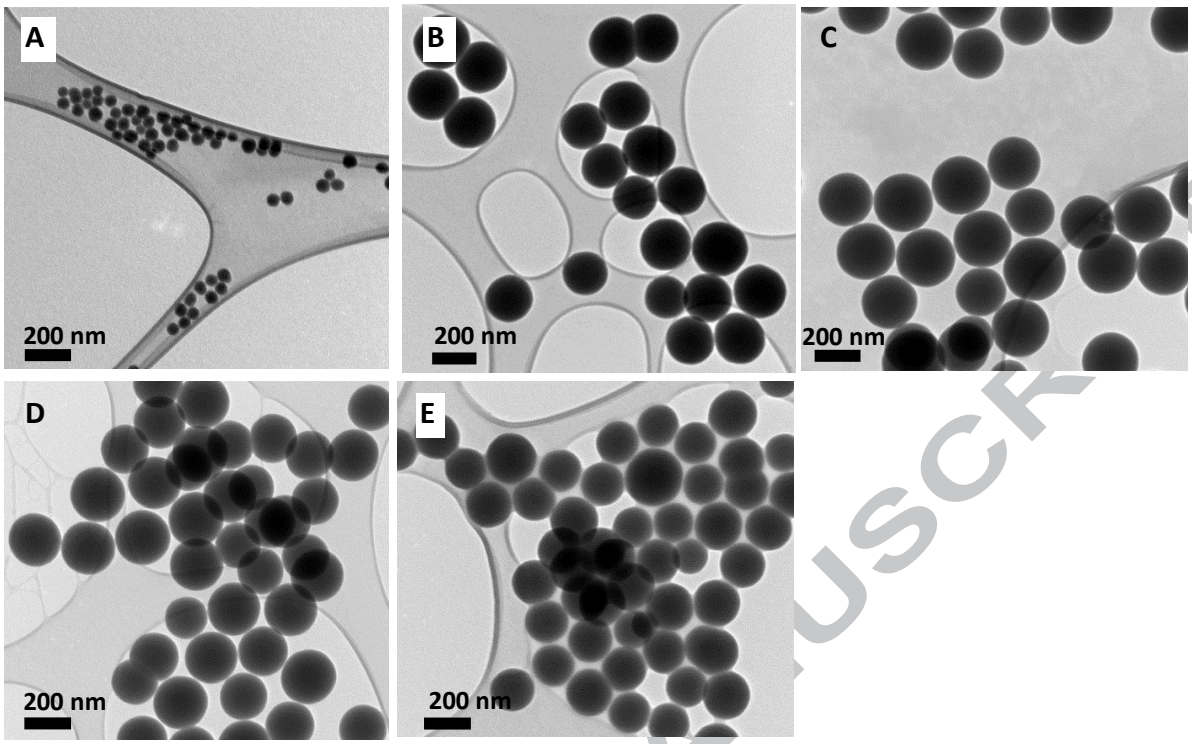

Figure 3. TEM images of silica particles produced using 0.28 M TEOS, 0.28 M NH_4OH and varying concentrations of water: A) 3 M H_2O B) 6 M H_2O C) 9 M H_2O D) 12 M H_2O E) 15 M H_2O.

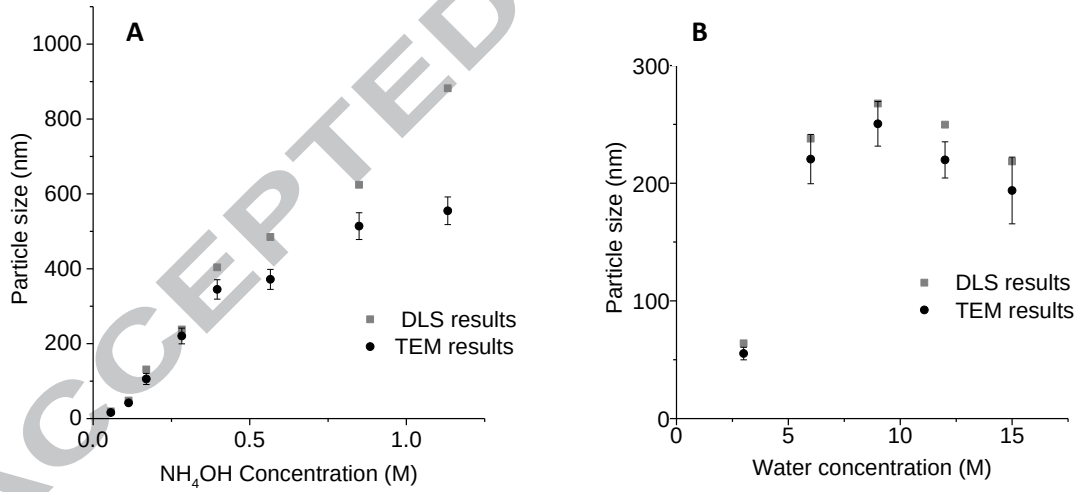

Figure 4. A comparison of DLS (number mean) and TEM results for silica particles showing variation of mean particle size with: A) ammonium hydroxide concentration for 0.28 M TEOS and 6 M H_2O and B) water concentration for 0.28 M TEOS and 0.28 M NH_4OH. Error bars for TEM results show the standard deviation of particle size in each sample (n=100).

Particle size measurements from TEM (Figure 4A) show that particle size increased linearly (R^2 = 0.9997) as ammonium hydroxide concentration increased, from 42.0 ± 5.5 nm at 0.11 M NH_4OH to 344.9 ± 25.9 nm at 0.40 M NH_4OH, before starting to level off. This trend was observed by both TEM and DLS characterisation methods, although the levelling off was less pronounced in DLS. For particle sizes in excess of 500 nm, we found that DLS no longer gave an accurate reading and instead tends to significantly overestimate particle size. Previous work analysing silica particles showed DLS to be accurate, although a maximum size of 400 nm was

used [36]. This unreliability of DLS at larger particle sizes is in agreement with Figure 1, which shows an increase in standard deviation of particle size from the mean as particle size increased, whilst the particles themselves remained monodispersed. The standard deviation for the TEM results shown in Figure 4 was calculated from 100 particles measured. The same sample was analysed in DLS to give a direct comparison. DLS gave a polydispersity index (PDI) of < 0.05 for the majority of samples indicating that samples were monodispersed. The standard deviation is not shown in Figure 4 for DLS results as the low PDI suggests that the particles are highly monodispersed.

Particle size variation was less sensitive to changes in water concentration. In the range 6 – 15 M H_2O, particle size measurements from TEM (Figure 4B) show that the mean diameter varied by less than 60 nm (for 0.28 M NH_4OH). However, there was an initial increase in mean diameter to 250.5 ± 18.9 nm at 9 M H_2O. At 0.28 M NH_4OH, for concentrations of water varying from 3 – 15M, the particle size remained below 300 nm and thus DLS gave reliable results. The particle size calculated by DLS was always slightly higher than TEM due to the fact that DLS measures the hydrodynamic radius.

The effect of variation of TEOS concentration was also investigated. Concentrations of 0.045 M, 0.17 M, 0.28 M and 0.5 M TEOS were chosen as these have been used most widely in literature [6, 8, 15, 35]. Water concentration was kept constant at 6 M and ammonium hydroxide concentration was varied between 0.11 and 0.57 M. At these concentrations the particle size remains within the limits of DLS and therefore this method was used for characterisation.

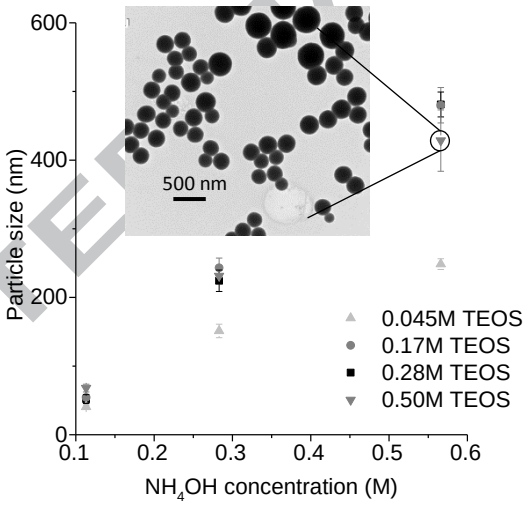

Figure 5. Mean particle size of silica particles (number mean from DLS) as a function of ammonium hydroxide concentration for 6 M H_2O and increasing TEOS concentrations. Error bars show the standard deviation of mean size (n=3). Inset shows heterodispersed particles at high TEOS and NH_4OH concentrations.

Increasing TEOS concentration from 0.045 M to 0.17 M resulted in an increase in particle size (Figure 5), although further increasing the concentration to 0.28 M resulted in no further size increase. However, increasing TEOS concentration directly resulted in an increased yield. For 20 ml total volume of solution, 0.17 M TEOS (0.17 M NH_4OH, 6 M H_2O) gave a dried nanoparticle mass of 229.7 ± 3.8 mg (n=3), whereas 0.28 M TEOS (0.17 M NH_4OH, 6 M H_2O) resulted in a corresponding 40% increase in yield, producing 384.7 ± 2.5 mg (n=3) dried mass of nanoparticles. Further increasing the TEOS to 0.5 M resulted in a further increase in yield, however particle size was less consistant, giving higher standard deviations and often polydispersed particles at high ammonium hydroxide concentrations. The PDI's for these particles (0.5M TEOS, 6M H_2O, 0.57M NH_4OH) ranged from 0.024 (monodisperse) to 0.618 (polydisperse). Thus for all further investiagations, 0.28 M was chosen as the optimum TEOS concentartion, giving a high yield and consistantly monodispersed particles.

Other papers have also observed heterodispersed particles at high TEOS and ammonium hydroxide concentrations [8].

3.2. Calcium incorporation

Previous work has shown that calcium only incorporates into the silicate network above 400°C, by diffusion and subsequent disruption of the silicate network as it becomes a network modifier [5]. Therefore, here, calcium nitrate was added only after the silica particles had formed. The hypothesis was that the calcium nitrate would deposit onto the surface of the particles during drying and then diffuse into the particles as temperature increased above 400°C. DLS and TEM data after heating to 680°C confirmed that the addition of calcium did not affect the size or morphology of the particles produced. This was true for all Si:Ca ratios, unlike recent methods [1]. However, TEM showed the washing step to be essential (Figure 6). EDX was used to confirm that areas of particles after drying (Figure 6B) were surrounded by excess calcium-rich phase, which was removed by washing in ethanol (Figure 6C). High resolution TEM (HRTEM) images of the resulting particles (Figure 7) show that they appear to have a homogeneous morphology with no crystalline areas. Nitrogen sorption measurements showed no porosity or significant differences in the specific surface area (BET method) of 100 nm SiO_2-CaO particles (23.6 m^2g^{-1}) compared to 100 nm Stober particles (28.0 m^2g^{-1}). These values are in agreement with literature on SiO_2-CaO nanoparticles which shows specific surface area to vary between 15-36 m^2g^{-1} depending on particle size [26].

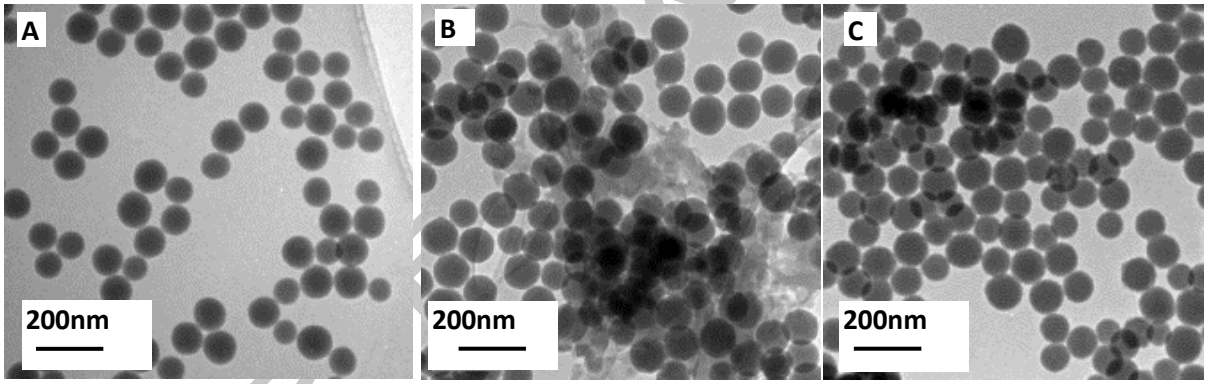

Figure 6. TEM images of silica particles (0.28 M TEOS, 0.17 M NH_4OH, 6 M H_2O) A) before the addition of calcium B) after the addition of calcium (Ca:Si ratio of 1.3:1) and heating to 680˚C) after subsequent washing in ethanol.

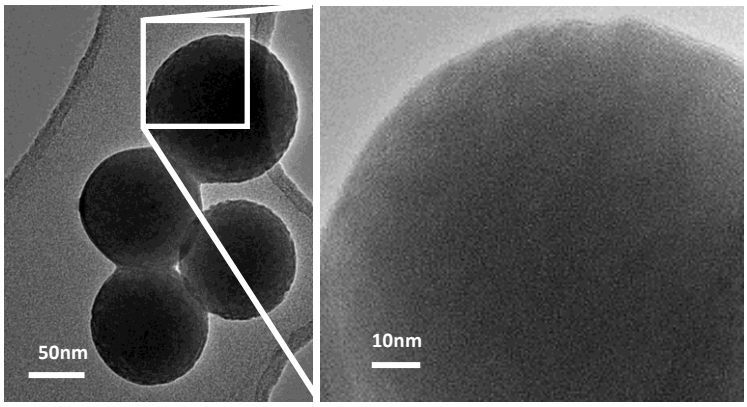

Figure 7. HRTEM of 100 nm silica particles (0.28 M TEOS, 0.17 M NH_4OH, 6 M H_2O) with Ca:Si added in the ratio 1.3:1 (after and heating to 680˚C and subsequent washing in ethanol)

Not all of the calcium added was incorporated into the particles, therefore analytical quantification post processing was required. Previous studies that report only the nominal concentrations of particles may therefore

have reported artificially high concentrations of calcium. It is also thought that the absence of this washing step in previous work will have led to higher concentrations of calcium reported [1].

Incorporation of calcium in 100 nm particles (0.28 M TEOS, 6M H_2O, 0.17 M NH_4OH) as a function of mol% Ca added to the solution, relative to 100 mol% Si, is shown in Figure 8, including EDX, XRF and ICP results. Adding the nominal amount of calcium (for composition 70S30C) gave only 3.7 ± 1.2 mol% of CaO incorporation due to the calcium not being incorporated into the silicate network at low temperatures and much of the calcium nitrate being removed in the supernatant. Excess unincorporated calcium-rich phase was also washed off in the washing step. ICP analysis of compositions show that for 100 nm particles, the addition of in calcium with the Ca:Si ratio of 1.3:1 gave a composition of 8.9 ± 1.1 mol% CaO, 91.1% SiO_2, which was confirmed by XRF. This ratio was found to be optimal in that further increasing the Ca:Si ratio to 2:1 and 4:1 resulted in no further increase in calcium incorporation. EDS also showed optimal calcium incorporation at a Ca:Si ratio of 1.3:1, therefore this ratio was used to synthesise all future particles.

Increasing the particle size, by increasing ammonium hydroxide concentration (Ca:Si ratio of 1.3:1), also resulted in a decrease in calcium incorporation. This supported our hypothesis for calcium incorporation occurring by diffusion at elevated temperature, as larger particles have a smaller surface area to volume ratio and diffusion distances from the surface are greater. For 500 nm particles (0.28 M TEOS, 0.57 M NH_4OH and 6 M H_2O) the addition of calcium in the Ca:Si ratio of 1.3:1 only gave 5.4 ± 1.3 mol % CaO according to ICP analysis.

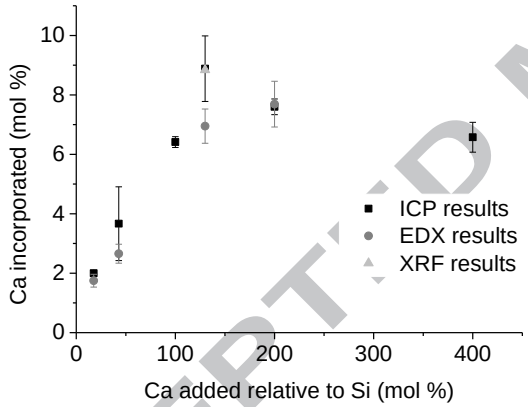

Figure 8. Incorporation of calcium in 100 nm particles (0.28 M TEOS, 6 M H_2O, 0.17 M NH_4OH) as a function of mol% Ca added to the solution relative to 100 mol% Si.

The hypothesis for calcium incorporation in to the silicate network was also supported by X-ray diffraction data (Figure 9) for particles both before and after heating. A broad feature ~ 1.6 $Å^{-1}$ was present for all samples. Smaller Bragg peaks at 1.4 and 1.8 $Å^{-1}$ were present for the sample containing calcium before heating (Figure 9C). These peaks were ascribed to calcium nitrate [43] and the absence of these peaks following heating (Figure 9D) is indicative of calcium nitrate decomposition and calcium entering the silicate network [31]. Silica particles without calcium were completely amorphous both before and after heating, as expected.

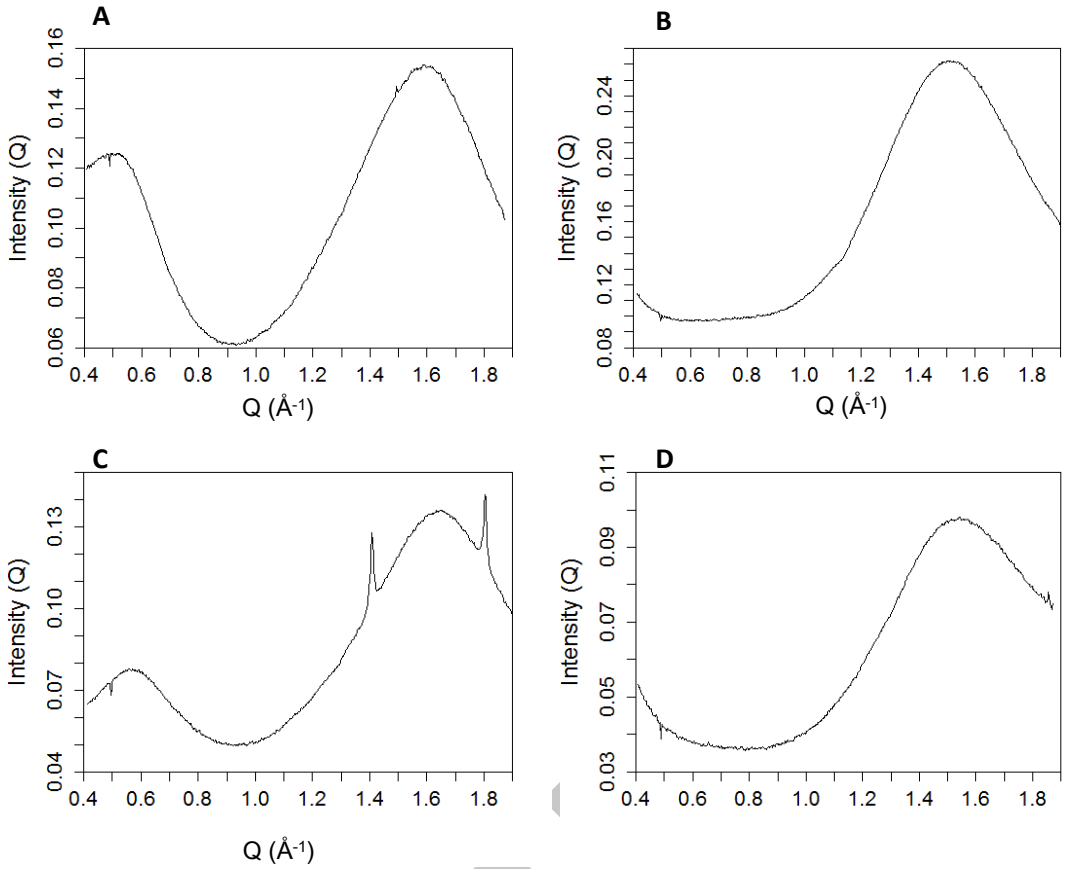

Figure 9. X-ray diffraction data for 100 nm particles (0.28 M TEOS, 6 M H_2O, 0.17 M NH_4OH): (A) silica particles, after drying at 60°C; (B) silica particles, heated to 680˚C; (C) SiO_2-CaO particles (synthesised with 0.28 M TEOS, 0.17 M NH_4OH, 6 M H_2O and a Ca:Si ratio of 1.3:1) after drying at 60°C and (D) SiO_2-CaO particles heated to 680˚C.

The ^{29}Si MAS NMR spectra for the Ca-free and Ca-incorporated Stöber particle systems are shown in Figure 10, with the chemical shift and integrated intensity data (measured via simulation) from these spectra reported in Table 1. These data show a reduction in Q^4 species after calcium incorporation, and a corresponding increase in Q^1, Q^2 and Q^3 species, reducing the number of bridging oxygen bonds and the network connectivity from 3.85 in pure silica particles to 3.68 in those containing 9% Ca. Theoretical network connectivity of glasses is often calculated from their composition using the equation[44]:

$$NC_{Si\ particles\ doped\ with\ Ca} = \frac{NC_{Si\ particles}\ [SiO_2] - 2[CaO]}{[SiO_2]}$$

The decrease in network connectivity (NC) obtained from the NMR data corresponds to a theoretical incorporation of 7.8% Ca as a network modifier, further validating compositional analysis results. Assuming a theoretical NC of 4 for pure SiO_2, then a theoretical NC of 3.80 would result from a nominal composition of 91% SiO_2, 9% CaO. However, the NC measured by NMR was lower in both types of particle since these systems also contain OH groups meaning that the H^+ can be considered an additional network modifier.

As the Ca enters the Stöber particles it should (in principle) disrupt the structure and thus act as a network modifier resulting in reduced overall connectivity (i.e. mean number of bridging oxygen bonds per silicon tetrahedral unit). In Ca containing bioactive glasses, it has been previously demonstrated that the effect of Ca^{2+} incorporation and the subsequent charge balancing required to stabilise the network can, in some cases, cause an upfield displacement of the ^{29}Si isotropic chemical shifts of the Q species by up to ~10 ppm. For example, mesoporous bioactive glass systems can accommodate 25 mol % CaO (or greater) and the large influence of Ca

on the immediate coordination sphere of each Si position is characterised by Q species shifts of Q^3_{Ca} ~ -90 ppm, Q^2_{Ca} ~ -83ppm and Q^1_{Ca} ~ -75 ppm [45]. Similar influences on the ^{29}Si MAS NMR shifts have been observed for sol-gel derived bioactive glass with CaO:SiO_2 ratios approaching ~50 mol% [46]. The shifts obtained in this work are reported in Table 1. They are representative of conventional Q speciation and clearly differ from those representative of large amounts of Ca incorporation and network modification. As evidenced by the ^{29}Si MAS NMR spectra (Figure 10) and the measured parameters (Table 1), the Ca incorporation into the Stöber particle systems is minimal (<10% maximum) which is too small to have a measurable influence on the shifts.

Table 1. Q distributions obtained from single pulse ^{29}Si MAS NMR spectra for silica and SiO_2-CaO (Ca:Si ratio of 1.3:1) particles synthesised with 0.28 M TEOS, 0.1 7M NH_4OH, 6 M H_2O heated to 680°C.

Sample	Q^1		Q^2		Q^3		Q^4		Network Connectivity (NC)
	δ_{Iso} [ppm]	I [%]	δ_{Iso} [ppm]	I [%]	δ_{Iso} [ppm]	I [%]	δ_{Iso} [ppm]	I [%]	
Stöber, Si particle	-	-	-91.7±0.1	2.9±0.4	-101.3±0.1	9.0±0.6	-110.5±0.1	88.1±0.1	3.85±0.02
Si particles doped with Ca	-80.5±0.9	1.8±0.2	-93.1±1.3	7.2±1.3	-100.5±0.2	12.0±1.4	-110.5±0.1	79.0±0.2	3.68±0.05

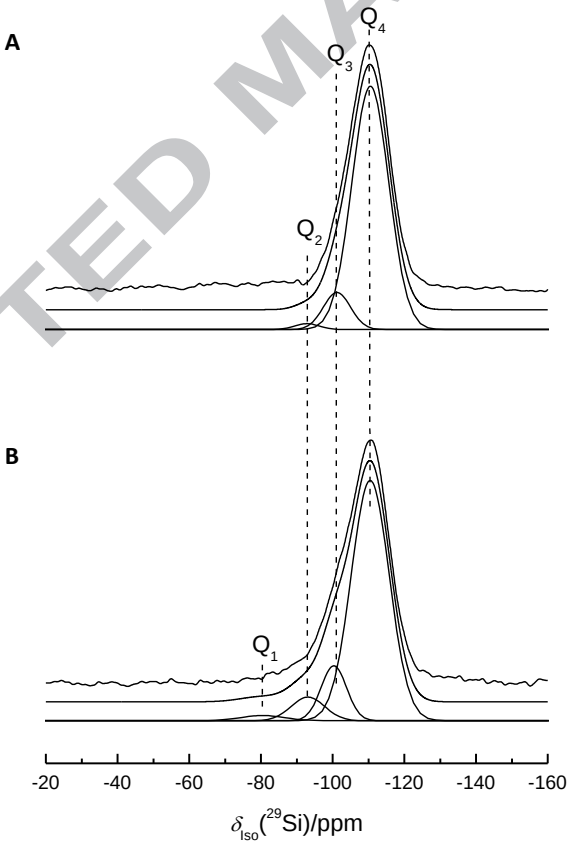

Figure 10. ^{29}Si MAS NMR spectra for 100 nm particles (0.28 M TEOS, 6 M H_2O, 0.17 M NH_4OH) heated to 680°C (A) silica and (B) SiO_2-CaO particles synthesised with Ca:Si ratio of 1.3:1.

For the first time, this paper also demonstrates that the calcium was present throughout the entire particles and not just near the surface. This was done by sectioning particles of 500 nm in diameter using FIB to produce a slice. After thinning, the resulting slice was electron transparent and therefore confirmed to be <100 nm thick. The monodispersity of the sample means that it could be confirmed that the section was through the centre of

the particle. Elemental mapping was performed using AZtec imaging software (Figure 11). Calcium, silicon and oxygen were present throughout the entire cross-section of the particle. No diffusion gradient was observed, confirming that the thermal treatment was sufficient to achieve homogeneity. It is assumed that as smaller particles will have a shorter diffusion distance, calcium will therefore penetrate throughout all the particles prepared and analysed in this paper. The calcium content of the smaller particles was also higher.

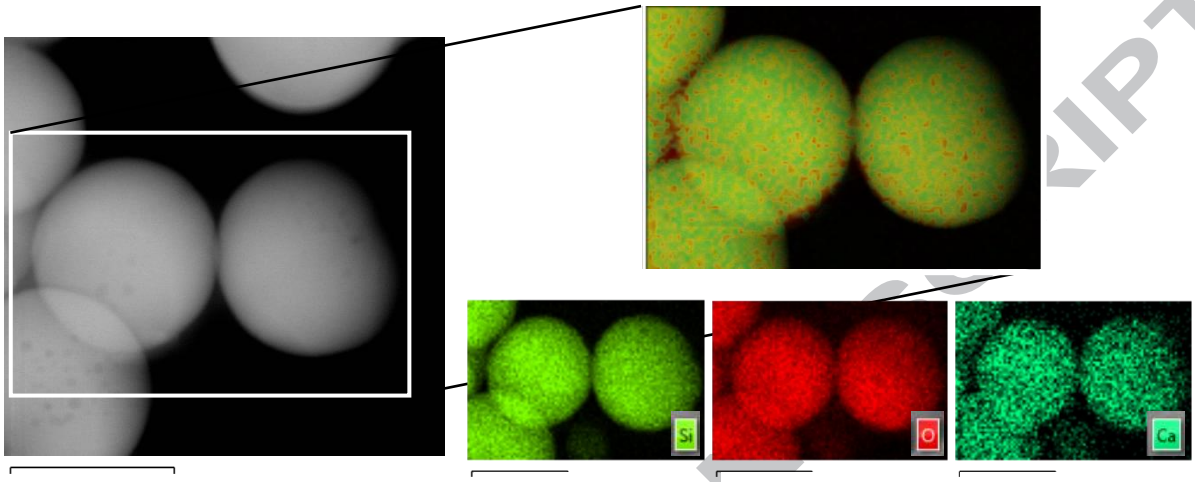

Figure 11. Distribution of elements through FIB cross sections of 500 nm particles of composition 94.6 mol% SiO_2, 5.4 mol% CaO, using AZtec imaging software on TEM.

3.3. Dissolution

Soluble silica and calcium ion release from the 100 nm particles in ALF and SBF over 2 weeks immersion are shown in Figure 12A and B. Dissolution begins with cation exchange between Ca^{2+} from the particles and H^+ ions from the solution, which then allows for some loss of soluble silica. Silica release occurs in both the silica and SiO_2-CaO particles because the silica network is not fully dense (as shown in the NMR data), due to H^+ ions also acting as network modifiers. This is why the incorporation of calcium did not affect silica release (Fig. 12A). In ALF, calcium was released steadily up to 1 week with a significant increase seen between 1 and 2 weeks for particles containing CaO. Silica release in SBF was higher than in ALF, due to the higher pH, which promotes the breaking of Si-O-Si bonds. In SBF, the calcium release (data not shown) was difficult to detect as Ca levels in SBF were high (~90 $\mu g ml^{-1}$) and the calcium is likely to have been released and redeposited (suggested by an observed decrease in P levels for SBF containing SiO_2-CaO particles). TEM images of SiO_2-CaO particles after 2 weeks immersion in ALF and SBF are shown in Figure 12D and E respectively. The morphology of pure silica particles (not shown) remained unchanged in both SBF and ALF, however dissolution of the particles containing calcium can be seen in ALF (Figure 12D). This calcium release is suggestive of potential bioactivity and indicates that the bioactive glass nanoparticles are likely to degrade inside lysosomes.

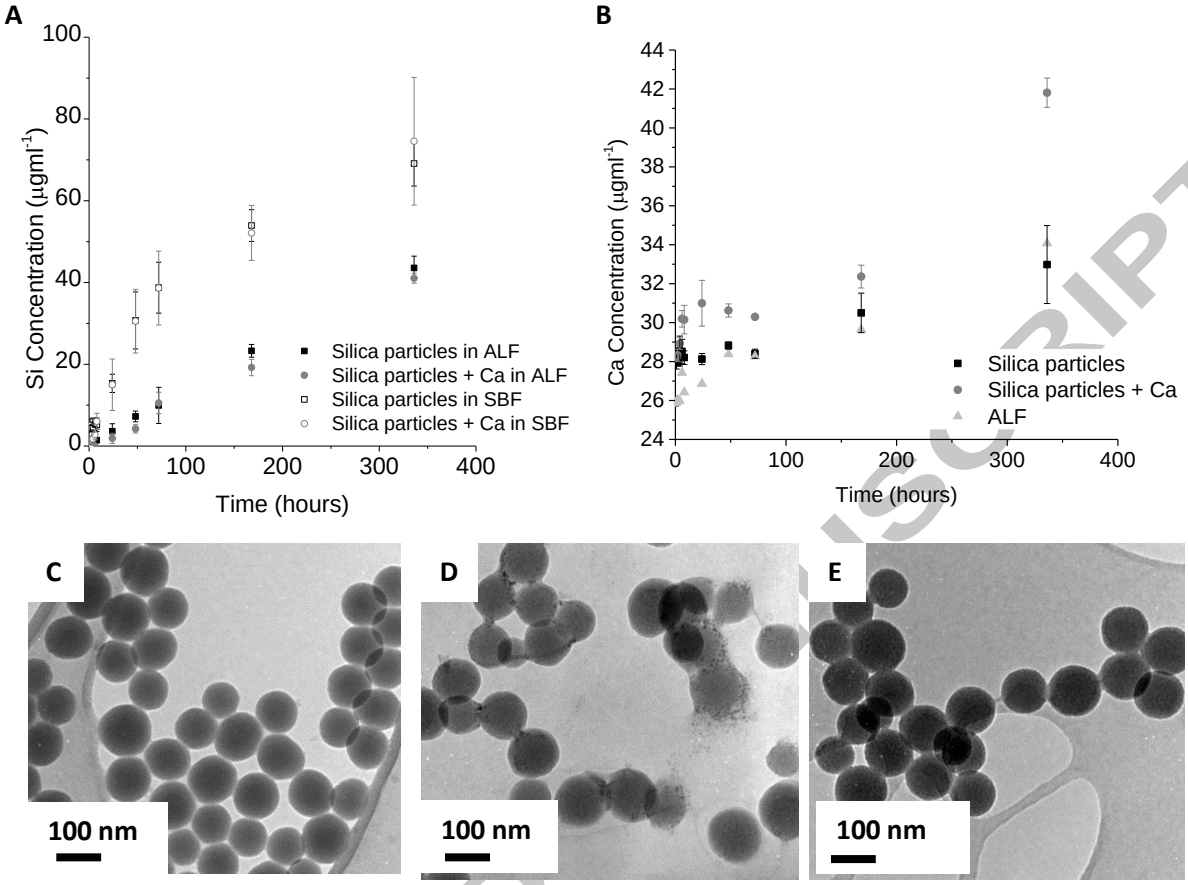

Figure 12. Dissolution study results in ALF and SBF from silica particles and SiO_2-CaO (Ca:Si ratio of 1.3:1) particles made with 0.28 M TEOS, 0.17 M NH_4OH, 6 M H_2O. (A) [Si] in ALF and SBF ; (B) [Ca] in ALF (C) TEM images of SiO_2-CaO particles before dissolution (D) TEM images of SiO_2-CaO particles after 2 weeks in ALF (E) TEM images of SiO_2-CaO particles after 2 weeks in SBF.

4. Conclusions

Spherical monodispersed particles were synthesised reproducibly with control of the modal size using a simple version of the original Stöber process. The particle size was tightly controlled through concentration of reactants. The modal particle size could be selected within the range of 20 – 500 nm. Ammonium hydroxide concentration had the largest effect on particle size and provided the best control, with increased ammonium hydroxide concentration increasing particle size. Particle size also increased as water concentration increased to 9 M, after which a decrease in size was observed as water was increased further. Decreasing the TEOS concentration from 0.28 – 0.17 M did not affect particle size or its distribution. However, reducing it to 0.045 M produced a smaller particle size and lower yield. TEM validated the use of DLS to analyse particle sizes up to 500 nm. However, beyond this size, DLS results are less consistent and tend to significantly overestimate the size of particles. The simple single step process gives good control of monodispersed particle size. There are many reports in the literature of more complicated methods that did not give improved control.

We also developed a method for incorporation of calcium into the silicate network while maintaining monodispersity and particle size control and identified the maximum limit of calcium incorporation. There are several reports in the literature of calcium containing silicate particles made by modification of the Stöber process, however the particles are often agglomerated with limited control of size. We have shown that the previous studies are likely to have overestimated the amount of calcium present in the composition. This is because calcium, from a calcium nitrate precursor, diffuses into the particles only during heating (above 400°C). We identified the optimal heating regime for calcium incorporation (heating to 680˚C) that did not affect size, dispersity or morphology of the particles and also maintained the amorphous structure. However, not all of the

calcium enters the particles so a washing step was required before composition analysis. A ratio of 1.3:1 Ca:Si is found to be optimal, giving a maximum of 8.9 ± 1.1 mol% CaO in the particles. Calcium incorporates throughout the particles homogeneously, disrupting the silica network and resulting in reduced network connectivity such that the particles degrade in ALF. Future work would involve investigating how calcium incorporates into the nanoparticles when other precursors are used, particularly calcium alkoxides.

Acknowledgements

The authors acknowledge the EPSRC (EP/I020861/1 and EP/M004414/1) and the Department of Materials, Imperial College London, for funding. J.V.H. also thanks the EPSRC and the University of Warwick for partial funding of the solid-state NMR infrastructure at Warwick, and acknowledge additional support for this infrastructure obtained through Birmingham Science City: Innovative Uses for Advanced Materials in the Modern World (West Midlands Centre for Advanced Materials Projects 1 and 2), with support from Advantage West Midlands (AWM) and partial funding by the European Regional Development Fund (ERDF). RAM would like to acknowledge STFC for funding a Global Challenge studentship.

References

[1] Tsigkou O, Labbaf S, Stevens MM, Porter AE, Jones JR. Monodispersed bioactive glass submicron particles and their effect on bone marrow and sdipose tissue-derived stem cells. Adv Healthc Mater. 2014;3:115-25.
[2] Hoppe A, Gueldal NS, Boccaccini AR. A review of the biological response to ionic dissolution products from bioactive glasses and glass-ceramics. Biomaterials. 2011;32:2757-74.
[3] Jones JR. Review of bioactive glass: from Hench to hybrids. Acta biomaterialia. 2013;9:4457-86.
[4] Brinker J, Scherer GW. Sol-gel science : the physics and chemistry of sol-gel processing. Boston: Academic Press; 1990.
[5] Lin S, Ionescu C, Pike KJ, Smith ME, Jones JR. Nanostructure evolution and calcium distribution in sol-gel derived bioactive glass. J Mater Chem. 2009;19:1276-82.
[6] Stober W. Controlled growth of monodisperse silica spheres in micron size range. Journal of Colloid and Interface Science 1968;26:62.
[7] Ab Rahman I, Padavettan V. Synthesis of Silica Nanoparticles by Sol-Gel: Size-Dependent Properties, Surface Modification, and Applications in Silica-Polymer Nanocomposites-A Review. J Nanomater. 2012.
[8] Bogush GH, Tracy MA, Zukoski CF. Preparation of monodisperse silica particles - control of size and mass fraction. Journal of Non-Crystalline Solids. 1988;104:95-106.
[9] Vanhelden AK, Jansen JW, Vrij A. Preparation and characterization of spherical monodisperse silica dispersions in non-aqueous solvents. Journal of Colloid and Interface Science. 1981;81:354-68.
[10] Matsoukas T, Gulari E. Dynamics of growth of silica particles from ammonia-catalyzed hydrolysis of tetra-ethyl-orthosilicate. Journal of Colloid and Interface Science. 1988;124:252-61.
[11] Branda F, Silvestri B, Luciani G, Costantini A. The effect of mixing alkoxides on the Stober particles size. Colloid Surf A-Physicochem Eng Asp. 2007;299:252-5.
[12] Green DL, Lin JS, Lam YF, Hu MZC, Schaefer DW, Harris MT. Size, volume fraction, and nucleation of Stober silica nanoparticles. Journal of Colloid and Interface Science. 2003;266:346-58.
[13] Harris MT, Brunson RR, Byers CH. The base-catalyzed-hydrolysis and condensation-reactions of dilute and concentrated TEOS solutions. J Non-Cryst Solids. 1990;121:397-403.
[14] Park SK, Do Kim K, Kim HT. Preparation of silica nanoparticles: determination of the optimal synthesis conditions for small and uniform particles. Colloid Surf A-Physicochem Eng Asp. 2002;197:7-17.
[15] Rao KS, El-Hami K, Kodaki T, Matsushige K, Makino K. A novel method for synthesis of silica nanoparticles. Journal of Colloid and Interface Science. 2005;289:125-31.

[16] Vanblaaderen A, Vangeest J, Vrij A. Monodisperse colloidal silica spheres from tetraalkoxysilanes - particle formation and growth-mechanism. Journal of Colloid and Interface Science. 1992;154:481-501.
[17] Feeney PJ, Napper DH, Gilbert RG. Coagulative nucleation and particle-size distributions in emulsion polymerization. Macromolecules. 1984;17:2520-9.
[18] Lee KT, Sathyagal AN, McCormick AV. A closer look at an aggregation model of the Stober process. Colloid Surf A-Physicochem Eng Asp. 1998;144:115-25.
[19] LaMer V, Dinegar R. Theory, production and mechanism of formation of monodispersed hydrosols. JACS. 1950;72:4847-54.
[20] Hench LL, Polak JM. Third-generation biomedical materials. Science. 2002;295:1014-7.
[21] Xynos ID, Edgar AJ, Buttery LDK, Hench LL, Polak JM. Gene-expression profiling of human osteoblasts following treatment with the ionic products of Bioglass (R) 45S5 dissolution. J Biomed Mater Res. 2001;55:151-7.
[22] Marelli B, Ghezzi CE, Mohn D, Stark WJ, Barralet JE, Boccaccini AR, et al. Accelerated mineralization of dense collagen-nano bioactive glass hybrid gels increases scaffold stiffness and regulates osteoblastic function. Biomaterials. 2011;32:8915-26.
[23] Labbaf S, Tsigkou O, Mueller KH, Stevens MM, Porter AE, Jones JR. Spherical bioactive glass particles and their interaction with human mesenchymal stem cells in vitro. Biomaterials. 2011;32:1010-8.
[24] Xia W, Chang J. Preparation and characterization of nano-bioactive-glasses (NBG) by a quick alkali-mediated sol-gel method. Mater Lett. 2007;61:3251-3.
[25] Luz GM, Mano JF. Preparation and characterization of bioactive glass nanoparticles prepared by sol-gel for biomedical applications. Nanotechnology. 2011;22:494014.
[26] Nedelec J-M, lao j, Lacroix J, Lukowiak A. Bioactive Glass Nanoparticles through Sol-Gel Chemistry. Chemical Communications. 2013.
[27] Hong ZK, Luz GM, Hampel PJ, Jin MS, Liu AX, Chen XS, et al. Mono-dispersed bioactive glass nanospheres: Preparation and effects on biomechanics of mammalian cells. J Biomed Mater Res Part A. 2010;95A:747-54.
[28] Hong Z, Liu A, Chen L, Chen X, Jing X. Preparation of bioactive glass ceramic nanoparticles by combination of sol-gel and coprecipitation method. J Non-Cryst Solids. 2009;355:368-72.
[29] Zhao Y, Zou H, Shi W, Tang L. Preparation and characterization of mesoporous silica spheres with bimodal pore structure from silica/hyperbranched polyester nanocomposites. Microporous and Mesoporous Materials. 2006;92:251-8.
[30] Rocha de Oliveira AA, de Souza DA, Silveira Dias LL, de Carvalho SM, Mansur HS, Pereira MdM. Synthesis, characterization and cytocompatibility of spherical bioactive glass nanoparticles for potential hard tissue engineering applications. Biomed Mater. 2013;8.
[31] Yu BB, Turdean-Ionescu CA, Martin RA, Newport RJ, Hanna JV, Smith ME, et al. Effect of Calcium Source on Structure and Properties of Sol-Gel Derived Bioactive Glasses. Langmuir. 2012;28:17465-76.
[32] Jones JR, Tsigkou O, Coates EE, Stevens MM, Polak JM, Hench LL. Extracellular matrix formation and mineralization of on a phosphate-free porous bioactive glass scaffold using primary human osteoblast (HOB) cells. Biomaterials. 2007;28:1653-63.
[33] Midha S, Kim TB, van den Bergh W, Lee PD, Jones JR, Mitchell CA. Preconditioned 70S30C bioactive glass foams promote osteogenesis in vivo. Acta Biomater. 2013;9:9169-82.
[34] Midha S, van den Bergh W, Kim TB, Lee PD, Jones JR, Mitchell CA. Bioactive glass foam scaffolds are remodelled by osteoclasts and support the formation of mineralized matrix and vascular networks in vitro. Adv Healthc Mater. 2013;2:490-9.
[35] Green DL, Lin JS, Lam Y-F, Hu MZC, Schaefer DW, Harris MT. Size, volume fraction, and nucleation of Stober silica nanoparticles. Journal of colloid and interface science. 2003;266:346-58.

[36] Bell NC, Minelli C, Tompkins J, Stevens MM, Shard AG. Emerging techniques for submicrometer particle sizing applied to Stober silica. Langmuir : the ACS journal of surfaces and colloids. 2012;28:10860-72.
[37] Hammersley AP, Svensson SO, Thompson A. Calibration and correction of spatial distortions in 2D detector systems. Nuclear Instruments and Methods in Physics Research Section A: Accelerators, Spectrometers, Detectors and Associated Equipment. 1994;346:312-21.
[38] Harris RK, Becker ED, Cabral de Menezes SM, Goodfellow R, Granger P. NMR nomenclature. Nuclear spin properties and conventions for chemical shifts (IUPAC Recommendations 2001). Pure and Applied Chemistry. 2001;73:1795-818.
[39] Bailey MM, Gorman EM, Munson EJ, Berkland C. Pure insulin nanoparticle agglomerates for pulmonary delivery. Langmuir. 2008;24:13614-20.
[40] Marques MRC, Loebenberg R, Almukainzi M. Simulated biological fluids with possible application in dissolution testing. Dissolut Technol. 2011;18:15-28.
[41] Kokubo T, Kushitani H, Sakka S, Kitsugi T, Yamamuro T. Solutions able to reproduce in vivo surface-structure changes in bioactive glass-ceramic A-W. Journal of biomedical materials research. 1990;24:721-34.
[42] Van Helden AK, Jansen JW, Vrij A. Preparation and characterization of spherical monodisperse silica dispersions in nonaqueous solvents. Journal of colloid and interface science. 1981;81:354-68.
[43] FitzGerald V, Martin RA, Jones JR, Qiu D, Wetherall KM, Moss RM, et al. Bioactive glass sol-gel foam scaffolds: Evolution of nanoporosity during processing and in situ monitoring of apatite layer formation using small- and wide-angle X-ray scattering. J Biomed Mater Res Part A. 2009;91A:76-83.
[44] Hill RG, Brauer DS. Predicting the bioactivity of glasses using the network connectivity or split network models. Journal of Non-Crystalline Solids. 2011;357:3884-7.
[45] Leonova E, Izquierdo-Barba I, Arcos D, López-Noriega A, Hedin N, Vallet-Regí M, et al. Multinuclear Solid-State NMR Studies of Ordered Mesoporous Bioactive Glasses. The Journal of Physical Chemistry C. 2008;112:5552-62.
[46] Lin Z, Jones JR, Hanna JV, Smith ME. A multinuclear solid state NMR spectroscopic study of the structural evolution of disordered calcium silicate sol-gel biomaterials. Physical Chemistry Chemical Physics. 2015;17:2540-9.

Graphical abstract